Cell Reports

Article

Inherent preference for polyunsaturated fatty acids instigates ferroptosis of Treg cells that aggravates high-fat-diet-related colitis

Graphical abstract

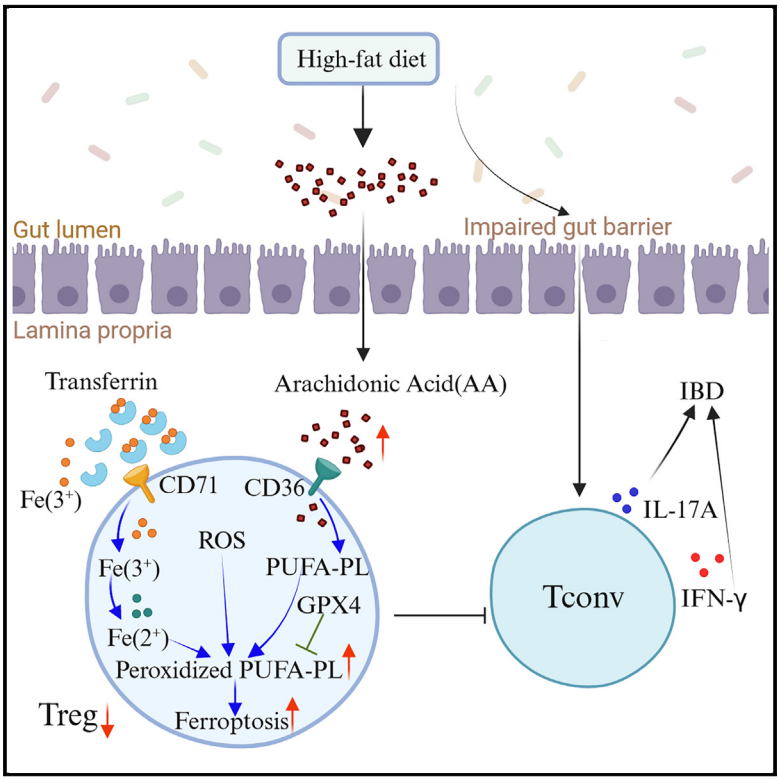

Highlights

- Intestinal Treg cells are more vulnerable than Tconv in HFD-induced ferroptosis
- Treg cells have intrinsic preference for using PUFA-PLs as membrane phospholipids
- High content of arachidonic acid in HFD aggravates ferroptosis of intestinal Treg cells
- GPX4 and a-tocopherol protect Treg cells against ferroptosis and HFD-related colitis

Authors

Junjie Yan, Yingying Zeng, Zerong Guan, ..., Yi-Fang Li, Rong-Rong He, Guangchao Cao

Correspondence

zhimin@mail.sysu.edu.cn (M.Z.), tzhinan@jnu.edu.cn (Z.Y.), wanyangsun@jnu.edu.cn (W.-Y.S.), liyifang706@jnu.edu.cn (Y.-F.L.), rongronghe@jnu.edu.cn (R.-R.H.), gccao2016@jnu.edu.cn (G.C.)

In brief

Yan et al. show that Treg cells have intrinsic preference for using PUFA-PLs as membrane phospholipids compared with Tconv. Therefore, the high content of PUFAs such as arachidonic acid in HFD aggravate ferroptosis of intestinal Treg cells, which might be one of the driving causes for HFD-related colitis.

Yan et al., 2024, Cell Reports *43*, 114636
August 27, 2024
https://doi.org/10.1016/j.celrep.2024.114636

CellPress

Cell Reports

CellPress
OPEN ACCESS

Article

Inherent preference for polyunsaturated fatty acids instigates ferroptosis of Treg cells that aggravates high-fat-diet-related colitis

Junjie Yan,[1,2,3,12] Yingying Zeng,[1,2,4,12] Zerong Guan,[1,2,3,12] Zhenhua Li,[5,12] Shunchang Luo,[6,12] Jie Niu,[7,12] Junzhang Zhao,[8,12] Haibiao Gong,[7] Ting Huang,[9] Zhongzhen Li,[1] Anyi Deng,[1,2,3] Qiong Wen,[1,2,3] Jingyi Tan,[1,2,3] Jun Jiang,[1] Xiucong Bao,[10] Sitao Li,[6] Guodong Sun,[11] Min Zhang,[8] Min Zhi,[8,*] Zhinan Yin,[1,2,3,*] Wan-Yang Sun,[7,*] Yi-Fang Li,[7,*] Rong-Rong He,[7,*] and Guangchao Cao[1,2,3,13,*]

[1]Guangdong Provincial Key Laboratory of Tumor Interventional Diagnosis and Treatment, Zhuhai Institute of Translational Medicine, Zhuhai People's Hospital (Zhuhai Clinical Medical College of Jinan University), Jinan University, Zhuhai 519000, China
[2]State Key Laboratory of Bioactive Molecules and Druggability Assessment, The Biomedical Translational Research Institute, Health Science Center (School of Medicine), Jinan University, Guangzhou 510632, China
[3]Key Laboratory of Viral Pathogenesis & Infection Prevention and Control (Jinan University), Ministry of Education, Guangzhou 510632, China
[4]Department of Laboratory Medicine, Nanfang Hospital Baiyun Branch, Southern Medical University, Guangzhou 510420, China
[5]Department of Systems Biomedical Sciences, School of Medicine, Jinan University, Guangzhou, China
[6]Department of Pediatrics, the Sixth Affiliated Hospital, Sun Yat-sen University, Guangzhou, China
[7]Guangdong Engineering Research Center of Chinese Medicine & Disease Susceptibility, Jinan University, Guangzhou 510632, China
[8]Department of Gastroenterology, the Sixth Affiliated Hospital, Sun Yat-sen University, Guangzhou 510632, China
[9]Department of Clinical Pathology, the First Affiliated Hospital of Jinan University, Guangzhou 510632, China
[10]School of Biomedical Sciences, Li Ka Shing Faculty of Medicine, The University of Hong Kong, Hong Kong SAR, China
[11]Guangdong Provincial Key Laboratory of Spine and Spinal Cord Reconstruction, The Fifth Affiliated Hospital (Heyuan Shenhe People's Hospital), Jinan University, Heyuan 517000, China
[12]These authors contributed equally
[13]Lead contact
*Correspondence: zhimin@mail.sysu.edu.cn (M.Z.), tzhinan@jnu.edu.cn (Z.Y.), wanyangsun@jnu.edu.cn (W.-Y.S.), liyifang706@jnu.edu.cn (Y.-F.L.), rongronghe@jnu.edu.cn (R.-R.H.), gccao2016@jnu.edu.cn (G.C.)
https://doi.org/10.1016/j.celrep.2024.114636

SUMMARY

Inflammatory bowel disease (IBD) has high prevalence in Western counties. The high fat content in Western diets is one of the leading causes for this prevalence; however, the underlying mechanisms have not been fully defined. Here, we find that high-fat diet (HFD) induces ferroptosis of intestinal regulatory T (Treg) cells, which might be the key initiating step for the disruption of immunotolerance and the development of colitis. Compared with effector T cells, Treg cells favor lipid metabolism and prefer polyunsaturated fatty acids (PUFAs) for the synthesis of membrane phospholipids. Therefore, consumption of HFD, which has high content of PUFAs such as arachidonic acid, cultivates vulnerable Tregs that are fragile to lipid peroxidation and ferroptosis. Treg-cell-specific deficiency of GPX4, the key enzyme in maintaining cellular redox homeostasis and preventing ferroptosis, dramatically aggravates the pathogenesis of HFD-induced IBD. Taken together, these studies expand our understanding of IBD etiology.

INTRODUCTION

Inflammatory bowel disease (IBD) is characterized by a debilitating chronic recurrent inflammation and a severely dysfunctional epithelium. Due to the rapid changes of environment and lifestyle, the prevalence rate of IBD is increasing in recent years and becoming a worldwide health problem.[1] The etiology of IBD has not been fully clarified, which involves a myriad of interactions among multiple factors such as diet, genetics, infection, and immune system.[2–4] Among dietary factors, high-fat diet (HFD) is widely believed to have a close correlation with the development of IBD.[5] Although the exact mechanisms linking the Western diet and the risk of IBD have not been fully defined, some seemingly reasonable mechanisms have been proposed. Specifically, the Western diet is associated with changes in intestinal microbiota and epithelial barrier function, which trigger a proinflammatory environment.[5,6]

Multiple immune cell populations participate in triggering the proinflammatory environment in IBD. In contrast, regulatory T (Treg) cells, which always express high levels of FOXP3 and CD25, are functionally immunosuppressive and important for immune tolerance to restrict IBD.[7–9] Previous studies have revealed that HFD causes immune cell activation in the colon and small intestine with a significant reduction of $CD4^+$ $Foxp3^+$

Tregs.[10] The reduced Treg cells cannot limit the proinflammatory immune response, which exacerbates the development of IBD. But the mechanism for the reduction of Treg cells after HFD treatment is still unknown.

Compared with conventional effector T cells, Treg cells favor lipid oxidation for metabolism and energy, which could also yield higher levels of reactive oxygen species (ROS).[11,12] ROS are a risk factor for the peroxidation and damage of membrane polyunsaturated fatty acids (PUFAs) that lead to cell ferroptosis.[13] This unique mode of cell death is regulated by a variety of cell metabolic events, including mitochondrial activity, redox homeostasis, and iron, amino acid, lipid, and sugar metabolism.[13] Glutathione peroxidase 4 (GPX4) is a key selenide enzyme in maintaining cellular redox homeostasis and preventing ferroptosis, which uses glutathione (GSH) as a cofactor to reduce membrane phospholipid hydroperoxides.[14,15] Arachidonic acid (AA) and its esterifiable products are the main substrates of lipid peroxidation and the key to inducing ferroptosis.[16,17] PUFAs such as AA are enriched in Western diets[18] and were known to trigger ferroptosis and aggravate colitis.[19,20] The goal of the study is to explore the etiology of HFD-related colitis. We hypothesized that the high levels of AA or its metabolic precursors in the Western diet and the intrinsic preference for lipid metabolism in Tregs might drive ferroptosis, and reduction of this immunosuppressive cell population might disrupt the immunotolerance in intestinal mucosa with ensuing colitis.

In this work, we revealed that Treg cells favor lipids for metabolism and prefer PUFAs for the synthesis of phospholipids. Consumption of an HFD, which contains high levels of PUFAs such as AA and its precursors, cultivates vulnerable Treg cells that are fragile to lipid peroxidation and ferroptosis. Since HFD also induces dysbiosis of the intestinal microbiota and increases the permeability of the intestinal barrier, this triggers the activation of resident immune cells.[6] The vigorous redox metabolism after activation generates high levels of ROS that instigate lipid peroxidation and ferroptosis of Treg cells, which disrupts the immunotolerance and increases the risk for colitis. We also found that GPX4 was reduced in colonic Treg cells after HFD treatment, and deleting *Gpx4* in Treg cells further exacerbated their ferroptosis and aggravated HFD-induced intestinal inflammation. Supplementing a-tocopherol could reverse the ferroptosis of Tregs and significantly ameliorated HFD-induced colitis. In summary, our work expanded our understanding on the etiology of IBD, identified a potential target in Treg cells in controlling immune balance, and provided a promising approach for the prevention of Western diet-related colitis.

RESULTS

High-fat diet induces ferroptosis of intestinal Treg cells

Western diet is a well-known risk factor for the pathogenesis of IBD, but the molecular mechanisms haven't been fully elucidated. We found that HFD treatment in mice significantly increased the production of proinflammatory cytokines from $CD4^+$ and $CD8^+$ T cells in the gut (Figures S1A and S1B) but reduced the percentage and amount of Treg cells (Figures 1A and S1C), a key immune-suppressive population in governing the homeostasis of intestinal immunity, which was consistent with previous reports.[10] To test whether the reduction of intestinal Treg cells was driven by ferroptosis, we detected the levels of ROS (CellRox Green), oxidized lipids (BODIPY FL C11, FITC/FITC + PE), and malondialdehyde (MDA, an end product of lipid peroxides) in intestinal T cells. We found that colonic Treg cells ($CD4^+$ $FOXP3^+$) exhibit slightly higher levels of ROS and lipid peroxides compared with conventional CD4 T cells (Tconv, $CD4^+$ $FOXP3^-$) under normal chow diet (NCD), and HFD treatment significantly potentiated lipid peroxidation in colonic Treg cells but not Tconv cells (Figures 1B–1D). HFD treatment induced more dramatic upregulation of lipid peroxidation in Tregs from small intestine, and it even potentiated lipid peroxidation and death of Tconv cells in the small intestine, albeit still much lower than Tregs (Figures S1D–S1F). This finding supports our hypothesis that HFD drives ferroptosis and reduction of Treg cells in the intestinal tract, since most dietary lipids are absorbed in the small intestine, and only a small amount of dietary lipids reach the colon. When analyzing the levels of GPX4, the key enzyme in maintaining cellular redox homeostasis and preventing ferroptosis, a selective impairment in colonic Tregs but not Tconv cells after HFD treatment was also detected (Figure 1E). Besides, colonic Treg cells also expressed higher levels of CD71, the transferrin receptor, than Tconv (Figure 1F), which was in concert with a previous report.[21] Moreover, HFD treatment indeed increased the death rate of Treg cells in both the colon and small intestine (Figures 1G and S1F). Transmission electron microscopy confirmed that the mitochondria of colonic Treg cells in the HFD group displayed slightly reduced size, and some of these mitochondria showed disrupted membrane and loss of cristae, which were typical morphological characteristics of ferroptosis (Figures 1H and 1I). Collectively, these results indicated that high fat consumption induced ferroptosis of intestinal Treg cells.

Treg cells favor lipid consumption and are more susceptible to arachidonic-acid-induced ferroptosis

Consumption of PUFAs, especially AA, increases the contents of PUFA-phospholipids (PUFA-PLs) in the membrane and the risk for ferroptosis.[19,20] Since HFD also contains high levels of PUFAs (Tables S1 and S2), we assumed that the ferroptosis of intestinal Tregs after HFD treatment might be due to the consumption of these lipids by Treg cells. Indeed, intestinal Treg cells expressed higher levels of CD36, a critical scavenger receptor required for lipid consumption and ferroptosis,[22,23] than Tconv cells (Figures 2A and S1G). After activation, Treg cells showed a persistent high level of CD36 (Figure 2B), consumed more lipids (Figure 2C), and thus had more lipid contents than Tconv cells (Figure 2D), which was consistent with previous reports describing that Treg cells favor lipids for energy and metabolism.[24–26] We next tested whether PUFAs, especially AA, could induce ferroptosis in Tregs. As shown in Figures S2A and S2B, supplementing AA in the culture medium induced much more severe cell death in Treg cells than the other PUFAs or monounsaturated fatty acid (MUFA), oleic acid (OA), or AA-treated Tconv cells. 40 μM AA was enough to elevate lipid peroxidation and death rates of Treg cells, and increasing AA dosage leads to further cell death. Supplementing OA reduced lipid peroxidation; however, overdose of OA was also toxic and

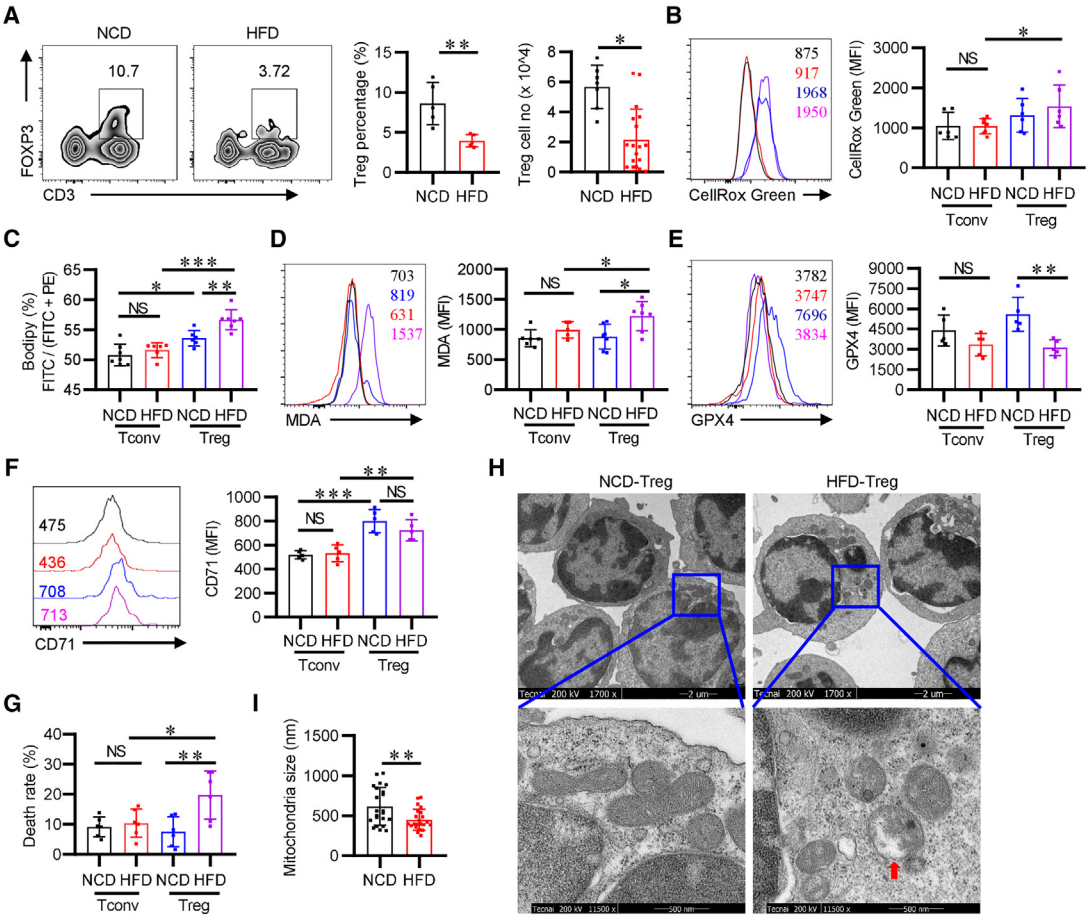

Figure 1. .High-fat diet induces ferroptosis of Treg cells but not conventional CD4$^+$ T cells in the colon

(A) C57BL/6J WT mice were fed with a normal chow diet (NCD) or high-fat diet (HFD) for 12 weeks. Representative fluorescence-activated cell sorting (FACS) plots (gated on CD45$^+$, left), percentage (middle, $n = 5$), and cell number (right, $n = 7$ for NCD and 18 for HFD) of Treg cells from the lamina propria of colon. (B–I) *Foxp3*$^{YFP-Cre}$ mice were fed with NCD or HFD for 12–16 weeks. The levels of ROS (CellRox Green, $n = 6$–7, B), BODIPY FL C11 ($n = 6$–7, C), malondialdehyde (MDA, $n = 5$–7, D), and GPX4 ($n = 5$, E) in Treg (CD4$^+$ FOXP3$^+$) or Tconv (CD4$^+$ FOXP3$^-$) cells from the lamina propria of colon were detected and shown. The levels of CD71 ($n = 5$, F) and the death rates (LIVE/DEAD$^+$, $n = 6$, G) in Treg (CD4$^+$ YFP$^+$) and Tconv (CD4$^+$ YFP$^-$) cells from the lamina propria of colon are shown. Transmission electron microscope images (H, scale bar represents 2 μm [upper] and 500 nm [lower]) and the statistical analysis of mitochondria size (I) of FACS-sorted colonic Treg cells (CD4$^+$ YFP$^+$) in NCD or HFD ($n = 22$, each dot represents a mitochondria). Data were mean ± SD. Two-tailed unpaired Student's t test (A and I) and one-way ANOVA with Tukey's multiple comparisons test (B–G). $p < 0.05$ (*), $p < 0.01$ (**), and $p < 0.001$ (***). NS, not significant. See also Figure S1.

the cause death of Treg cells (Figure 2E). Hereby, we used 40 μM AA for the subsequent experiments. In addition, the elevated oxidation of lipids and glutathione and increased death rate of Treg cells after AA treatment could be reversed by a ferroptosis-specific inhibitor Ferrostatin-1 (Fer-1) (Figures 2F, 2G, and S2C), which further supported that AA induced ferroptosis of Treg cells.

We then performed liquid chromatography-mass spectrometry (LC-MS)-based redox phospholipidomics analysis of Treg and Tconv cells treated with or without AA or OA to dissect the influence of these fatty acids on the oxidation of phospholipids, which is the molecular basis of ferroptosis. We found that there are inherent differences regarding the composition of phospholipids between Treg and Tconv cells, and adding AA or OA had more dramatic influences on the composition and oxidation of phospholipids in Treg cells than Tconv (Figures S2D and S2E). Specifically, Treg cells had an inherently higher level of PUFA-PLs but lower levels of MUFA-PL and saturated phospholipids (SFA-PLs) than Tconv. Adding AA enlarged these differences, while adding OA reversed the differences in PUFA-PLs and MUFA-PLs (Figure 2H). These results suggested that Treg cells have an inherent preference of using PUFA for the anabolic synthesis of membrane phospholipids compared with Tconv, but they could make faster adjustment than Tconv to adapt environmental lipid nutrient alterations. In line with the higher levels of PUFA-PLs, Treg cells contain more peroxidized phospholipids than Tconv, and this increase was further expanded to more peroxidized phospholipids after AA treatment (Figures 2I, 2J, and S2E–S2G). We next tested whether AA could induce lipid peroxidation and death in intestinal Tregs *in vivo* by adding AA in the diet. As expected, supplementing AA in NCD induced much higher levels of lipid peroxidation and cell death in colonic Treg

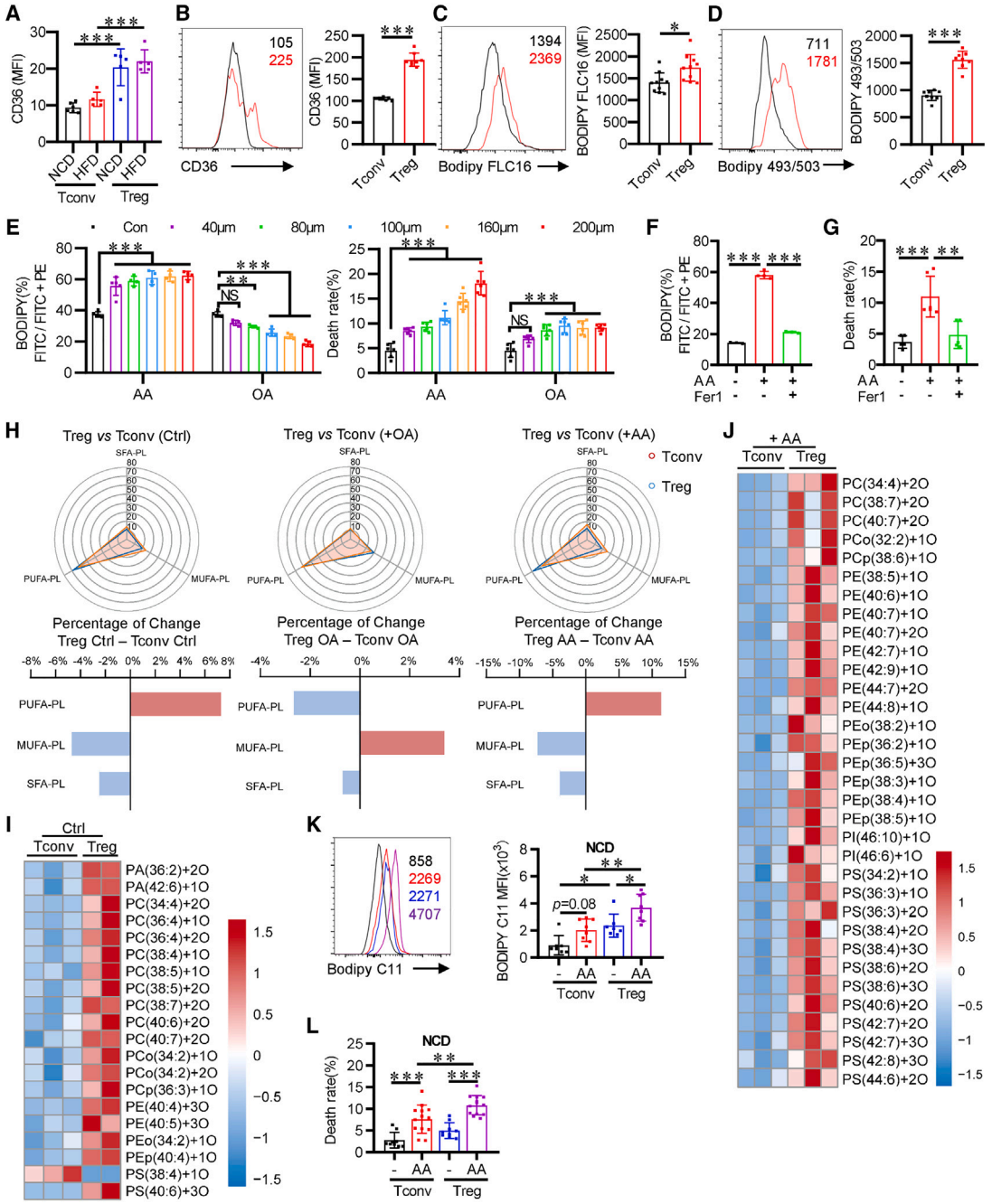

Figure 2. Treg cells favor lipid consumption and are more susceptible to arachidonic-acid-induced ferroptosis

(A) *Foxp3*$^{YFP-Cre}$ mice were fed with NCD or HFD for 12–16 weeks, and the levels of CD36 in colon Treg and Tconv cells were analyzed and are shown (n = 5–6).

(B–D) Splenic CD4$^+$ T cells from *Foxp3*$^{YFP-Cre}$ mice were stimulated with α-CD3 + α-CD28 + rmIL-2 for 24 h. The levels of CD36 (n = 8, B), BODIPY FL C16 consumption (n = 10, C), and cellular neutral lipid contents (BODIPY 493/503, n = 8, D) in Treg or Tconv cells were detected and are shown.

(E) Splenic CD4$^+$ T cells from *Foxp3*$^{YFP-Cre}$ mice were cultured in the presence of different concentrations of arachidonic acid (AA) or oleic acid (OA) for 48 h. The lipid oxidation (n = 4–5) and the death rates (n = 6) of Treg cells were detected and are shown.

(F and G) Splenic CD4$^+$ T cells from *Foxp3*$^{YFP-Cre}$ mice were cultured in the presence of AA (40 μM) with or without Fer-1 (20 μM) for 24 h. The lipid oxidation (n = 3–4, F) and the death rates (n = 5–6, G) of Treg cells were analyzed.

(H–J) Treg (CD4$^+$ YFP$^+$) and Tconv (CD4$^+$ YFP$^-$) cells were sorted from *in vitro* cultured splenic CD4$^+$ T cells that were primed under Treg or Tconv conditions, respectively. Sorted Treg or Tconv cells were then cultured in the presence of AA (40 μM) or OA (40 μM) for 48 h and used for LC-MS/MS-based lipidomics and redox phospholipidomics analysis of phospholipids and peroxidized phospholipids.

(legend continued on next page)

cells than Tconv (Figures 2K and 2L), which were consistent with the findings made *in vitro* (Figures S2A and S2B).

Taken together, the aforementioned findings converged to strongly support the conclusion that Treg cells favor lipid consumption and have a higher content of PUFA in membrane phospholipids, especially when encountering excessive AA, which makes them more vulnerable to peroxidation and ferroptosis.

Treg-specific *Gpx4*-deficient mice were healthy on normal chow but developed unrestrained intestinal inflammation after HFD treatment

Next, we figured whether Treg cell ferroptosis contributes to HFD-induced intestinal inflammation. As mentioned above, GPX4 is a key enzyme that inhibits ferroptosis. Thus, we generated Treg-specific *Gpx4*-deficient mice via crossing $Gpx4^{f/f}$ with $Foxp3^{YFP-Cre}$ strain to specifically potentiate ferroptosis in Treg cells. The rationale for this strategy was also in concert with the phenomenon that HFD treatment significantly reduced the expression of GPX4 in intestinal Treg cells (Figure 1E). Compared with $Foxp3^{YFP-Cre}$ littermate controls (wild type, WT), $Foxp3^{YFP-Cre}$ $Gpx4^{f/f}$ mice (knockout, KO) manifested normal body size and colon length at 15 weeks of age (Figures S3A and S3B). Histological analysis of the colon tissue also showed normal epithelial structure that contained massive goblet cells and abundant mucus in both $Foxp3^{YFP-Cre}$ and $Foxp3^{YFP-Cre}$ $Gpx4^{f/f}$ mice (Figure S3C). To characterize the immune features in the colon of $Foxp3^{YFP-Cre}$ $Gpx4^{f/f}$ mice, we isolated the lymphocytes from the lamina propria and dissected the immune compartments. We found that the percentage of Treg cells was slightly decreased in $Foxp3^{YFP-Cre}$ $Gpx4^{f/f}$ mice, but the overall quantity of Treg cells was comparable with WT littermates (Figure S3D). The production of IFN-γ and IL-17 from $CD4^+$ T cells was slightly increased (Figure S3E). Since IL-17 can effectively mediate the excitatory process of neutrophil mobilization and inflammatory response, we also measured the proportion and number of local neutrophils. As shown in Figure S3F, deficiency of *Gpx4* in Treg cells did not alter the infiltration of $CD11b^+$ $Ly6G^+$ neutrophils in the colon. We also performed redox phospholipidomic analysis of freshly isolated splenic GPX4-KO Treg cells and WT Tregs. Interestingly, GPX4-KO Treg cells contained slightly higher levels of PUFA-PLs and lower levels of SFA-PLs than WT Treg cells (Figure S3G). The oxidation levels for most of the phospholipids in GPX4-KO Tregs were comparable to WT Tregs except for a slight upregulation of monooxidized phosphatidylethanolamine plasmalogen PEp(42:6)+1O and monooxidized phosphatidylserine PS(36:2)+1O (Figure S3H), suggesting marginally elevated lipid oxidation. Collectively, these results indicated that Treg-specific *Gpx4*-deficient mice were healthy in appearance under normal diet albeit with a slight reduction of Tregs and disturbed production of inflammatory cytokines.

We then set these mice on HFD treatment. Surprisingly, $Foxp3^{YFP-Cre}$ $Gpx4^{f/f}$ mice were unable to gain body weight once switched to HFD and began to lose weight after a few weeks, and these mice were all dead within 13 weeks of HFD treatment (Figures 3A–3C). Henceforth, mice were sacrificed and analyzed after 6–8 weeks of HFD treatment. As expected, $Foxp3^{YFP-Cre}$ $Gpx4^{f/f}$ mice developed severe colitis compared with $Foxp3^{YFP-Cre}$ littermate controls as indicated by significantly shortened colon length (Figure 3D), thickened but unstructured epithelium, massive infiltration of lymphocytes (Figure 3E), decreased number of goblet cells, and reduced secretion of mucins (Figure 3F). HFD $Foxp3^{YFP-Cre}$ $Gpx4^{f/f}$ mice also showed more severe disruption of the colonic epithelial barrier compared with the HFD $Foxp3^{YFP-Cre}$ group as indicated by the increased permeability and the reduced expression of tight-junction-related genes (Figures 3G and 3H). Meanwhile, HFD $Foxp3^{YFP-Cre}$ $Gpx4^{f/f}$ mice also showed upregulation of proinflammatory cytokines and chemokines in the colon and elevated plasma levels of interleukin-6 (IL-6), IL-1β, and tumor necrosis factor alpha (TNF-α) (Figures 3I and 3J).

When analyzing the immune compartments in the colon, we found that HFD treatment induced a dramatic reduction of Treg cells after *Gpx4* deficiency (Figure 4A), while the proportion of $CD4^+$ and total amount of infiltrated $CD4^+$ or $CD8^+$ T cells were increased (Figures 4B and 4C). IL-17^+ $CD4^+$ effector T cells and neutrophils in the colon were also substantially increased, while the total amount and percentages of macrophages were largely unaffected (Figures 4D–4F). The percentages of IFN-γ^+ in colonic $CD4^+$ and $CD8^+$ T cells were comparable between the two groups, but the total number of IFN-γ-producing cells was still significantly increased (Figure 4D). HFD $Foxp3^{YFP-Cre}$ $Gpx4^{f/f}$ mice also showed significant reduction of Treg cells in the small intestine, together with disturbance of $CD4^+/CD8^+$ ratio and the increased proinflammatory cytokine production in $CD4^+$ T cells (Figure S4). These results clearly indicated that Treg-specific ferroptosis after *Gpx4* deficiency provoked unlimited intestinal inflammation in HFD condition that was detrimental to the enteric canal and even mortal.

An interesting phenomenon was that despite the much smaller and emaciated body, $Foxp3^{YFP-Cre}$ $Gpx4^{f/f}$ mice developed more severe hyperlipidemia after HFD treatment (Figure S5A). Serum from KO mice contained higher levels of triglyceride and low-density lipoproteins (LDLs) and lower levels of high-density lipoproteins (HDLs) (Figures S5B–S5D). Hyperlipidemia is a risk factor for myocardial damage; therefore, we performed histological analysis on the heart tissue of mice. Indeed, the heart tissues from KO mice exhibited obvious vacuolization (usually indicates increased fatty degeneration) (Figure S5E), disordered arrangement of myocardial cells, and infiltration of immune cells (Figure S5F), which might lead to myocardial weakness. The

(H) The radar plots and differences for the percentages of saturated phospholipids (SFA-PLs), monounsaturated phospholipids (MUFA-PLs), and polyunsaturated phospholipids (PUFA-PLs) in Treg and Tconv cells.

(I and J) The heatmap of oxidized phospholipids with differences between Treg and Tconv cells with (J) or without (I) AA treatment.

(K and L) Mice were fed with an NCD that was supplemented with or without extra AA (4 g/kg) for 9–10 weeks. The levels of lipid oxidation (n = 7–8, K) and death rates (n = 9–13, L) of Treg and Tconv cells in the lamina propria of colon were detected and are shown. Data were mean ± SD. Two-tailed unpaired Student's t test (B–D) and one-way ANOVA with Tukey's multiple comparisons test (A, E–G, K, and L). $p < 0.05$ (*), $p < 0.01$ (**), and $p < 0.001$ (***). NS, not significant. See also Figure S2.

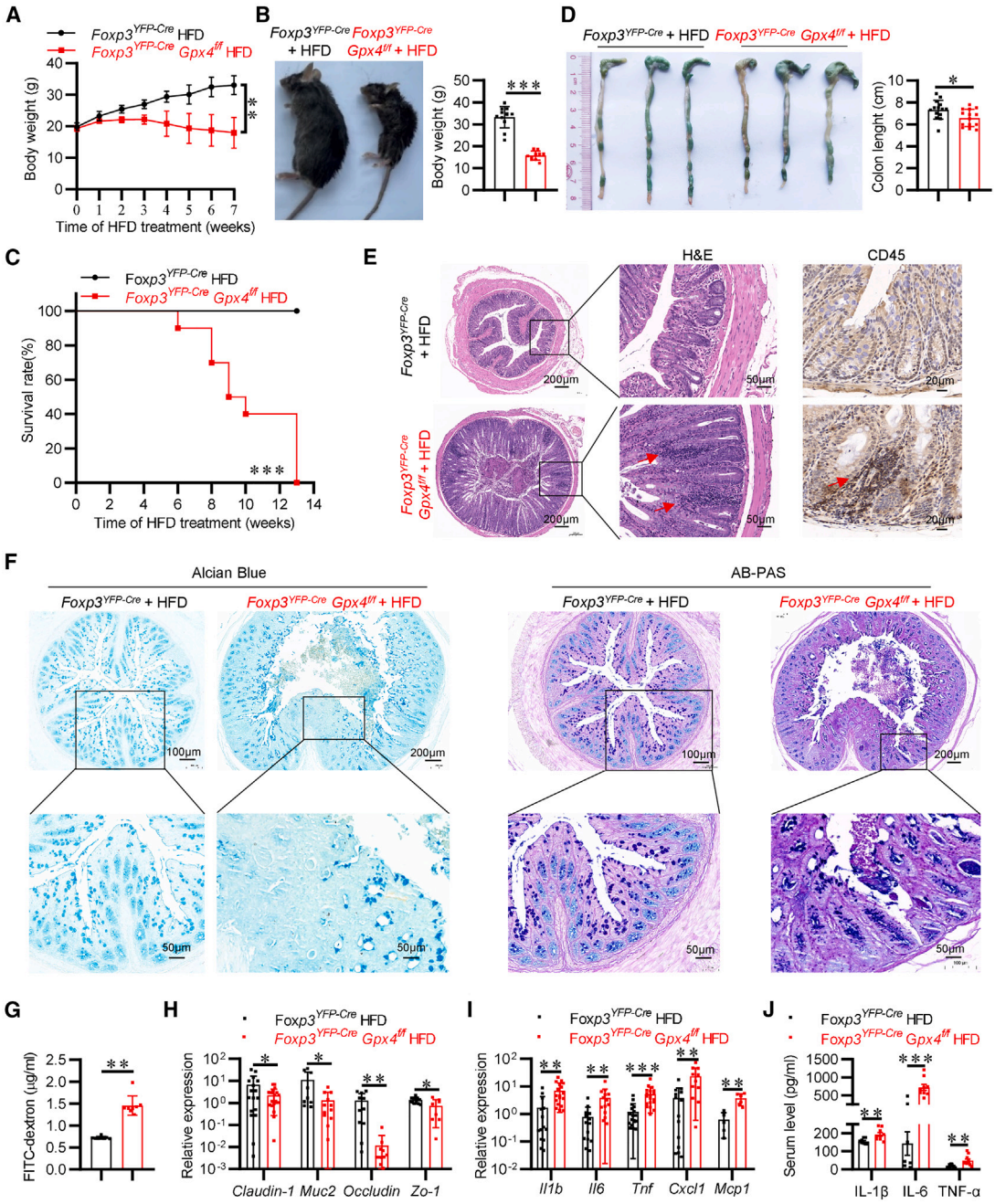

Figure 3. Treg-specific *Gpx4*-deficient mice developed severe colitis after HFD treatment

Foxp3$^{YFP-cre}$ *Gpx4*$^{f/f}$ and *Foxp3*$^{YFP-Cre}$ mice were fed an HFD for 7 (A, B, and D–J) or 13 (C) weeks.

(A) Body weight curve during HFD treatment (n = 6–7).

(B) Representative images and body weights after 7 weeks of HFD treatment (n = 10–12).

(C) The survival rates of mice after HFD treatment (n = 10–11).

(D) Representative images of colon tissue and statistical analysis of colon length (n = 14).

(E) Representative hematoxylin and eosin (H&E) staining (scale bar represents 200 μm [left] and 50 μm [right]) and CD45 staining (scale bar represents 20 μm) of colon tissues.

(F) Alcian blue and Alcian blue/periodic acid-Schiff (AB-PAS) staining of colon tissue (scale bar represents 100 μm or 200 μm [upper] and 50 μm [lower]).

(G) Mice were treated with FITC-dextran (4 kDa) via gavage, and the plasma was collected after 4 h. Plasma concentrations of FITC-dextran (4 kDa) were detected and are shown (n = 8).

(legend continued on next page)

remarkably increased serum triglycerides and LDL also increased the risk of developing myocardial infarction with ensuing tissue damage and release of lactate dehydrogenase (Figures S5G–S5H), and this might lead to the death of mice (Figure 3C). The underlying mechanism for the hyperlipidemia in these KO mice, however, needs further investigation.

Ferroptosis-induced death of Treg cells after GPX4 deficiency leads to impaired immune suppression

In order to exhibit immune suppressive function, Tregs cells need to be activated by T cell receptor (TCR) and co-stimulatory signals, which also mobilize rapid metabolism with tremendous redox reactions. Since Treg cells have an inherently higher level of PUFA-PLs (Figure 2H), we speculated that the ferroptosis may occur after the activation of Treg cells. Thus, Treg cells from *FOXP3*$^{YFP-Cre}$ WT mice were stimulated via TCR *in vitro* for activation and used for detection of ferroptosis. We found that both lipid peroxidation (MDA and BODIPY C11) and mortality of Treg cells were significantly increased after activation for 72 h, which could be partially reversed by adding Fer-1 (Figures S6A–S6C). Besides, the lipid peroxidation of *in vitro* activated Treg cells could also be reduced by Fer-1 or α-tocopherol (Figure S6D). These experiments suggested that ferroptosis participated in the death of Treg cells after activation via TCR *in vitro*. Then, we tested whether GPX4 protects Tregs from ferroptosis-induced cell death using Treg cells isolated from *Foxp3*$^{YFP-Cre}$ (WT) or *Foxp3*$^{YFP-Cre}$ *Gpx4*$^{f/f}$ (KO) mice. Since previous studies have revealed that the high oxygen level *in vitro* (i.e., 21%) was detrimental to GPX4-deficient T cells even under unstimulated condition,[27] Treg cultures without TCR stimulation were also performed in these experiments. We found that un-activated WT Treg cells died slowly *in vitro*, and TCR stimulation significantly accelerated this process (Figure S6E), which was consistent with the findings shown in Figures S6A–S6D. In line with previous studies on GPX4-deficient CD4 and CD8 T cells,[27] GPX4-KO Treg cells also died very quickly *in vitro* even in the absence of TCR stimulation; however, activation via TCR could still accelerate it (Figure S6E). Besides, GPX4-KO Treg cells also yielded higher levels of peroxidized lipids after *in vitro* activation (Figure S6F). These results suggested that both the hyperoxic *in vitro* environment and the activation-driven metabolic processes could induce ferroptosis of GPX4-KO Treg cells. The cell death could be restrained by the addition of Fer-1 or partially rescued by α-tocopherol (a liposoluble reductive agent that protects against lipid peroxidation) but not by z-VAD-FMK (zVAD, inhibitor for apoptosis) or necrostatin-1 (Nec-1, inhibitor for necroptosis) (Figures S6G and S6H), further supporting that the rapid death of GPX4-KO Tregs upon activation was due to ferroptosis. Collectively, the above results indicated that GPX4 deficiency sensitized Treg cells to ferroptosis-induced cell death.

We next checked the effects of GPX4 deficiency on the immunosuppressive function of Treg cells. In accordance with the dramatic cell death of GPX4-KO Tregs after TCR activation *in vitro* (Figure S6D), they almost completely lost the suppressive function in the *in vitro* suppressing assay (Figure S7A). We then evaluated the suppressive activity of *Gpx4*-deficient Treg cells *in vivo* after being co-transferred with naive CD4$^+$ T cells into *Rag1*$^{-/-}$ mice (Figure S7B). Transfer of naive CD4$^+$ T cells breaks the immune tolerance of *Rag1*$^{-/-}$ mice and induces colitis in a few weeks, while the co-transferred Treg cells will be mobilized to inhibit the inflammatory responses. As expected, *Gpx4*-deficient Treg cells also failed to protect *Rag1*-deficient mice from the development of colitis as indicated by the loss of weight, shorter colon length, and enlarged spleen (Figures S7C–S7E). 6 weeks post transfer, the transferred GPX4-KO Treg cells in the spleen were significantly less than WT Treg cells (Figure S7F), and therefore, they failed to suppress the inflammatory cytokine production from the transferred CD4$^+$ T cells (Figure S7G). These data revealed that the ferroptosis-induced death of Treg cells after GPX4 deficiency led to impaired immune suppression both *in vitro* and *in vivo*.

Vitamin E protects intestinal Treg cells from ferroptosis

Intestinal Treg cells in the *Foxp3*$^{YFP-Cre}$ *Gpx4*$^{f/f}$ mice were only marginally reduced, and the immunotolerance was largely intact under NCD (Figure S3), which indicated that the ferroptosis in these cells was less severe, and there were extra pathways to prevent lipid peroxidation beyond GPX4-mediated elimination of lipid hydroperoxides using glutathione. Vitamin E was known for protection against ferroptosis due to its reductive activity and liposolubility, and our previous data have shown that α-tocopherol (a derivate of vitamin E) could protect GPX4-KO Treg cells from lipid peroxidation and ferroptosis *in vitro* (Figures S6D, S6G, and S6H). Therefore, we speculated that vitamin E in NCD might also protect intestinal Treg cells from lipid peroxidation and ferroptosis, which preserved a fragile but still functional immunotolerance in *Foxp3*$^{YFP-Cre}$ *Gpx4*$^{f/f}$ mice.

To test this hypothesis, we eliminated vitamin E from the normal diet and fed both *Foxp3*$^{YFP-Cre}$ and *Foxp3*$^{YFP-Cre}$ *Gpx4*$^{f/f}$ mice for 5 weeks. As expected, *Foxp3*$^{YFP-Cre}$ *Gpx4*$^{f/f}$ mice developed more severe colitis compared with *Foxp3*$^{YFP-Cre}$ littermate controls as indicated by dramatic loss of body weight, increased mortality, thickened but unstructured epithelium, massive infiltration of lymphocytes, reduced goblets cells, and decreased expression of mucins (Figures S8A–S8D). When analyzing the immune compartments in the colon, we found that vitamin E deprivation induced dramatic reduction of Treg cells in *Foxp3*$^{YFP-Cre}$ *Gpx4*$^{f/f}$ mice (Figure S8E), while the proportion and amount of infiltrated CD4$^+$ and CD8$^+$ T cells were significantly increased (Figures S8F and S8G). The percentage of IL-17$^+$ CD4$^+$ effector T cells was also substantially increased, while the ratios of IFN-γ$^+$ in CD4$^+$ or CD8$^+$ effector T cells were either unaffected or slightly decreased (Figures S8H and S8I). However, the total amounts of IFN-γ$^+$ CD4$^+$, IL-17$^+$ CD4$^+$, and IFN-γ$^+$ CD8$^+$ effector T cells in the colon of *Foxp3*$^{YFP-Cre}$ *Gpx4*$^{f/f}$ mice

(H) Relative levels of mRNAs of intestinal permeability-related genes in the colon tissue (n = 8–21).
(I) Relative levels of mRNAs of inflammatory factor-related genes in the colon tissue (n = 5–19).
(J) Plasma concentrations of IL-1β, IL-6, and TNF-α were detected via ELISA (n = 7–14). Data were mean ± SD. Two-tailed unpaired Student's t test (B, D, and G–J), two-way ANOVA (A), and log rank test (C). $p < 0.05$ (*), $p < 0.01$ (**), and $p < 0.001$ (***). See also Figures S3 and S5.

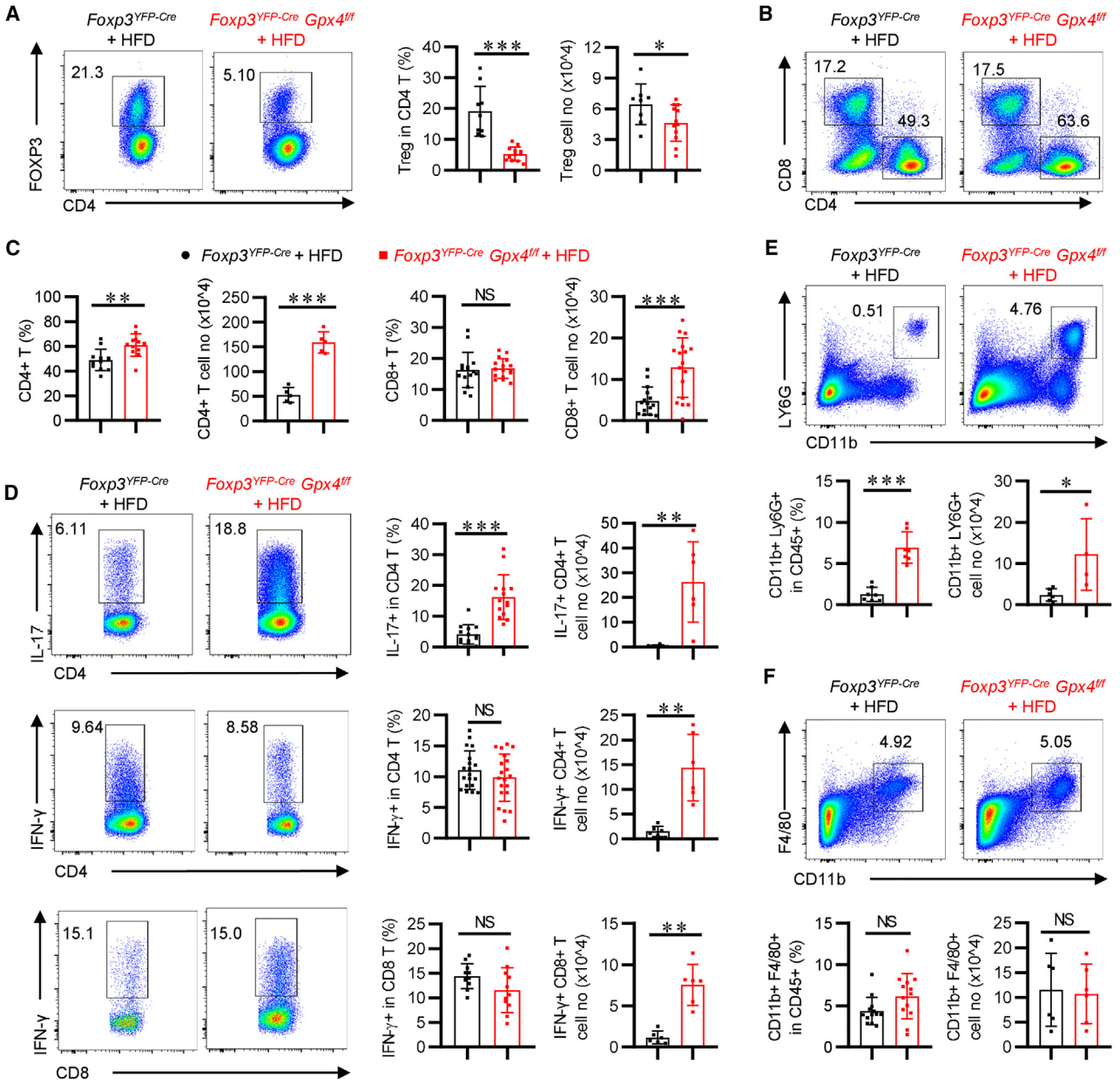

Figure 4. Treg-specific *Gpx4*-deficient mice displayed unrestrained inflammatory responses in the colon after HFD challenge

(A–F) *Foxp3*$^{YFP-cre}$ *Gpx4*$^{f/f}$ and *Foxp3*$^{YFP-Cre}$ mice were fed with HFD for 7 weeks. Lymphocytes in the lamina propria of colon tissues were isolated and used for analysis of immune compartments and cytokine production. Representative FACS plots and statistical analysis of the frequencies (n = 9–12) and quantities (n = 8–12) of Treg cells (A), CD4$^+$ (n = 12 for percentage, and n = 5 for cell number), and CD8$^+$ (n = 15–17) T cells (B and C), cytokine production (n = 6 for cell number, n = 13–14 for IL-17 in CD4, n = 19–20 for IFN-γ in CD4, and n = 11 for IFN-γ in CD8, D), CD11b$^+$ LY6G$^+$ neutrophils (n = 7 for percentages, and n = 4–6 for cell number, E), and CD11b$^+$ F4/80$^+$ macrophages (n = 13 for percentages, and n = 6 for cell number, F) are shown. Data were mean ± SD. Two-tailed unpaired Student's t test (A and C–F). $p < 0.05$ (*), $p < 0.01$ (**), and $p < 0.001$ (***). NS, not significant. See also Figures S4–S7.

were still increased due to the elevated amounts of CD4$^+$ and CD8$^+$ T cells (Figure S8J). These results clearly indicated that vitamin E plays an important role in protecting intestinal Treg cells against ferroptosis and preventing intestinal inflammation. It worth noting that vitamin E deprivation elicited more severe reduction of intestinal Treg cells and more rapid death of *Foxp3*$^{YFP-Cre}$ *Gpx4*$^{f/f}$ mice compared with HFD treatment (Figures 3C, 4A, S6B, and S6E), suggesting that vitamin E deprivation was more detrimental to GPX4-KO Tregs than HFD-elicited increase of PUFAs and antigens.

We than tested whether replenishing α-tocopherol could reverse the ferroptosis of GPX4-deficient Treg cells *in vivo* and protect the *Foxp3*$^{YFP-Cre}$ *Gpx4*$^{f/f}$ mice from colitis after HFD consumption. Excitingly, we found that supplementing α-tocopherol

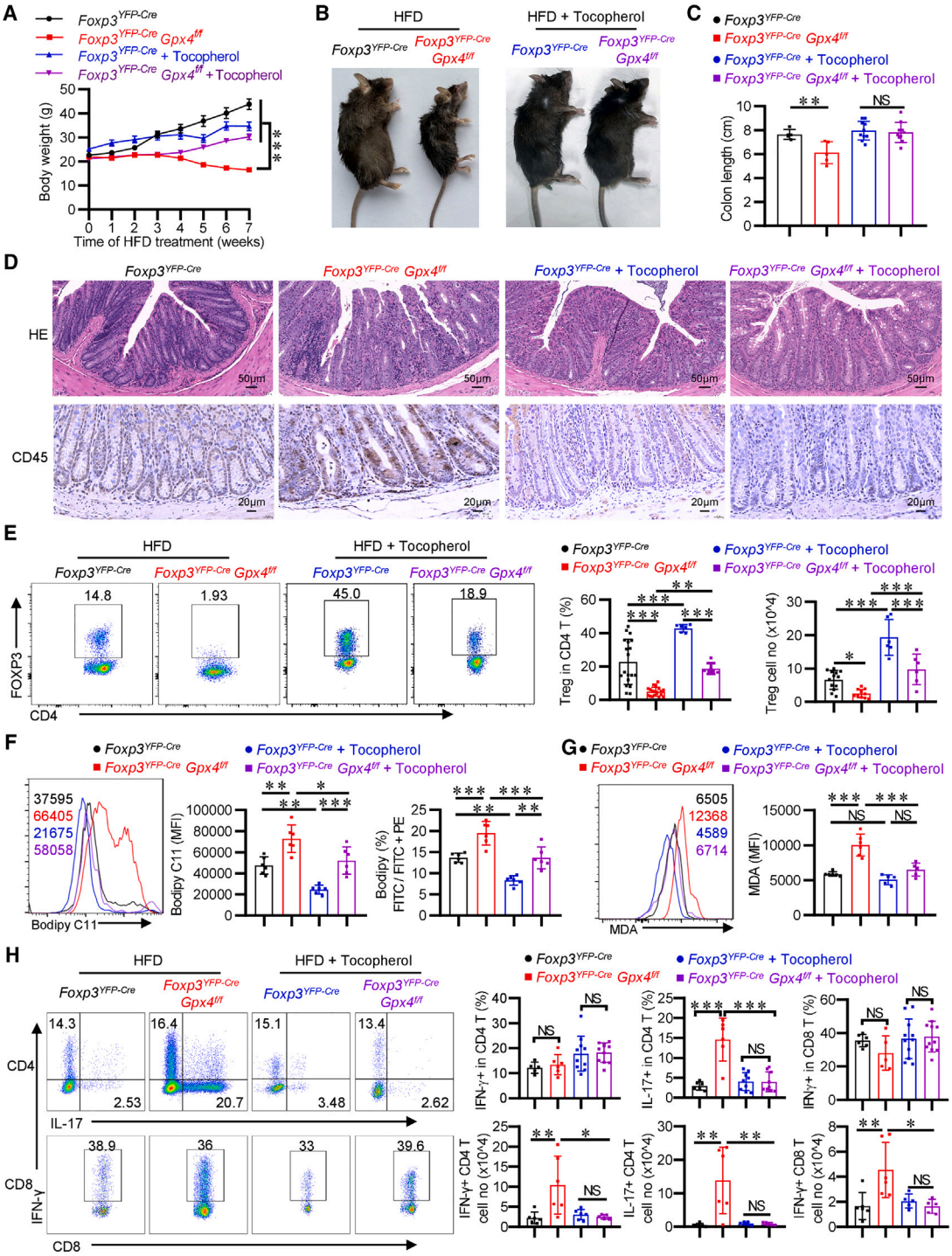

Figure 5. α-Tocopherol prevents HFD-induced colitis in *Foxp3*$^{YFP-cre}$ *Gpx4*$^{f/f}$ mice

Mice were treated with HFD or α-tocopherol-enriched HFD (0.5 g/kg) for 7 weeks.

(A–C) Body weights were recorded weekly (n = 5–6). Representative pictures (B) and colon lengths (n = 5–10, C) of mice after 7 weeks of treatment.

(D) Representative H&E staining (scale bar represents 50 μm) and CD45 staining (scale bar represents 20 μm) images of the colon.

(E–G) Lymphocytes in the lamina propria of colon tissues were isolated and used for analysis of immune compartments, lipid peroxidation, and cytokine production. Representative FACS plots and statistical analysis of the frequencies (n = 6–19) and quantities (n = 6–13) of Treg cells (E) are shown. Lipid peroxidation (Bodipy C11, n = 6, F) and MDA (n = 5–6, G) levels in Treg cells are shown.

(legend continued on next page)

almost completely reversed the susceptibility to HFD-induced colitis in *Foxp3*$^{YFP-Cre}$ *Gpx4*$^{f/f}$ mice as indicated by normal body weight, colon length, and intact epithelium structure without massive lymphocyte infiltration (Figures 5A–5D). The reduced cell number and increased lipid peroxidation of Treg cells in HFD-treated *Foxp3*$^{YFP-Cre}$ *Gpx4*$^{f/f}$ mice were also partially reversed after replenishing α-tocopherol (Figures 5E–5G). Meanwhile, supplementing α-tocopherol also restrained the elevated production of inflammatory cytokines (Figure 5H). Taken together, these data strongly indicated that replenishing α-tocopherol could reverse the GPX4-deficiency-derived Treg cell ferroptosis and colitis.

DISCUSSION

The incidence of IBD is increasing and has a close relationship with the Westernization of dietary habits, which are characterized with increased intake of fat.[1,6] However, the mechanism of high fat consumption in aggravating IBD has not been fully clarified. Previous studies have been focused on the dysbiosis of intestinal microbiota caused by the Western diet, which triggers the proinflammatory immune reactions.[6] But this does not explain the disruption of immune homeostasis—why "immunosuppression" fails under this condition. In 2015, Luck et al. reported that an HFD induces the activation of multiple immune cells in the colon but significant reduction of $CD4^+$ $Foxp3^+$ Tregs.[10] The loss of Treg cells could explain the failure of immunosuppression in HFD-related IBD; however, how HFD caused the reduction of Treg cells was still unknown.

In this work, we found that Treg cells express a higher level of CD36, a critical lipid scavenger, and have stronger ability to utilize external fatty acids than conventional T cells, which are in concert with their preference for lipid metabolism. These cells also favor PUFAs for the synthesis of membrane phospholipids; thus, they are more vulnerable to ROS-induced phospholipid peroxidation. Besides, Treg cells express a higher level of CD71 (the transferrin receptor) than Tconv and generate more ROS, and both increased the potential for ion-mediated Fenton reaction that leads to lipid peroxidation and ferroptosis. Since PUFAs, especially AA and its precursors, are prevalent in the Western diet (or more specifically in HFD),[18] a Westernized dietary habit will cultivate a fragile Treg cell population in the gut that contains high levels of PUFA-PLs and that can be easily destroyed by lipid peroxidation and ferroptosis. HFD consumption also induces dysbiosis of commensal microbiota and increases the permeability of the epithelial barrier,[6] thus augmenting the load of invading pathogens that trigger the activation of the immune system including Tregs. But the vigorous metabolism after activation will yield a large amount of ROS in Treg cells that drives peroxidation of PUFA-PLs. When losing protections that can eliminate lipid peroxides (such as dysfunction of GPX4 or deprivation of vitamin E), these fragile Treg cells will die and be unable to maintain immune tolerance, and this eventually leads to colitis. These results indicate that the inherent preference for lipid metabolism in Treg cells and the prevalence of PUFAs in the Western diet conspire to instigate Treg cell ferroptosis that disrupts immunotolerance and increases the risk for colitis. An interesting phenomenon is that HFD treatment also reduces the expression of GPX4 in colonic Treg cells (Figure 1E). It is conceivable that the reduction of GPX4 probably also contributes to the increased ferroptosis of Treg cells after HFD consumption; however, the underlying mechanism for this reduction needs further investigation.

In fact, HFD not only aggravates the pathogenesis of colitis, but it also increases the risk of a variety of inflammatory diseases such as hepatitis and diabetes, which also exhibited reduced levels of Treg cells.[28,29] Since PUFAs such as AA and its precursors can be directly absorbed in the intestine and transported into the circulation, it will be interesting to test whether ferroptosis also contributes to the reduction of Treg cells in these tissues. Besides, intestinal Treg cells can also migrate to the periphery and affect peripheral immune responses. Thus, it is also possible that the reduction of Treg cells in these tissues is due to less migration from the intestine.

HFD consumption is also a major driver for the development of obesity. HFD-induced obesity is accompanied by immune dysregulations that are characterized by chronic inflammation and increased risk for autoimmunity and inflammatory disorders but impaired adaptive immunity in vaccines[30] and cancers,[31,32] which seems to be the opposite. In fact, HFD induces dysbiosis of microbiota, disrupts barrier structure, and disturbs intestinal immune tolerance, all of which contribute to systemic chronic inflammation. Therefore, it is conceivable that the preactivation of proinflammatory immune cells in obesity promotes autoimmunity and inflammation. The impairment of adaptive immunity in vaccines and cancer of obese subjects, however, could be explained by the disturbed development and metabolism of T/B cells and the systemic changes of hormones that influence immune cell function.[30,33] Besides, chronic inflammation is also a risk factor in driving cancer. In addition, there are intense nutritional competitions in the tumor microenvironment. Previous studies have revealed that tumor cells and tumor-infiltrated Tregs express high levels of lipid metabolism-related genes to support their nutritional demands.[26,31] Therefore, the increased risk for inflammatory disorders and the impairment in vaccines or tumor in HFD-related obesity are not contradictory.

GPX4 is a key enzyme in protection against lipid peroxidation and ferroptosis. Its role in maintaining the homeostatic balance of T cells and in T cell-mediated anti-infection has been revealed.[27,34] Recently, Xu et al. reported that GPX4 promotes the survival of intra-tumoral Tregs to repress anti-tumor immunity,[35] which was in concert with the finding that tumor-infiltrating Treg cells favor fatty acid metabolism[24–26] and was consistent with our work. These studies also suggest that the lipid metabolism-GPX4-ferroptosis pathway has a broad impact on Treg cells, and again, this mechanism might be applicable to a variety of immune imbalances.

(H) Representative FACS plots and statistical analysis of the frequencies (n = 5–11) and quantities (n = 5–6) of cytokine-producing T cells. Data were mean ± SD. One-way ANOVA with Tukey's multiple comparisons test (C and E–H) and two-way ANOVA (A). $p < 0.05$ (*), $p < 0.01$ (**), and $p < 0.001$ (***). NS, not significant. See also Figure S8.

In summary, our work uncovered a novel mechanism for the etiology of Western diet-related IBD, identified a potential target in Treg cells in controlling immune homeostasis, and provided a promising approach for treating Western diet-related colitis.

Limitations of the study

The etiology of IBD is complicated. Both the imbalance of effector/regulatory immune cells and the disruption of pro-resolving mediators are involved in the pathogenesis of IBD.[36] However, this work didn't test whether HFD affects the release of pro-resolving mediators by T cells. Intestinal resident immune cells adapt their metabolism according to the substrate availability, and redox phospholipidomic analysis of intestinal Treg cells from mice under NCD or HFD treatment would provide more accurate characterization of peroxidized lipids to explain the ferroptosis and reduction of Treg cells under HFD. Unfortunately, redox phospholipidomic analysis requires a large amount of cells, but we could not gather enough intestinal Treg cells for this experiment. Another limit of this work is the lack of data on HFD-related human IBD, which are more valuable in clinic and should be characterized in the near future.

STAR★METHODS

Detailed methods are provided in the online version of this paper and include the following:

- KEY RESOURCES TABLE
- RESOURCE AVAILABILITY
  - Lead contact
  - Materials availability
  - Data and code availability
- EXPERIMENTAL MODEL AND STUDY PARTICIPANT DETAILS
  - Mice
- METHOD DETAILS
  - Lamina propria lymphocytes isolation
  - Flow cytometry
  - Histology
  - Quantitative real-time PCR
  - *In vitro* activation of T cells
  - *In vitro* fatty acid treatment
  - Suppression assay of treg cells
  - Preparation of treg cells for lipidomic analysis
  - LC-MS/MS-based phospholipidomics analysis
- QUANTIFICATION AND STATISTICAL ANALYSIS

SUPPLEMENTAL INFORMATION

Supplemental information can be found online at https://doi.org/10.1016/j.celrep.2024.114636.

ACKNOWLEDGMENTS

This work is supported by the National Key Research and Development Program of China (grant 2020YFA0803502 to Z.Y. and grant 2022YFC0867400 to R.-R.H. and Y.-F.L.), the Guangdong Basic and Applied Basic Research Foundation (grant 2023B1515020018 to G.C. and grant 2023B0303000004 to G.C. and Z.Y.), the National Natural Science Foundation of China (grants 31830021 and 32030036 to Z.Y., 81670477 to M. Zhi, and 32200079 to Z.L.), Guangdong Provincial Key Laboratory of Tumor Interventional Diagnosis and Treatment (grant 2021B1212040004 to Z.Y.), the Innovation Team Project of Guangdong Provincial Department of Education (2023KCXTD003 to Z.Y. and G.C. and 2020KCXTD003 to R.-R.H. and Y.-F.L.), Guangzhou Municipal Science and Technology Bureau (grant 2024A04J6326 to G.C.), the Health and Medical Research Fund (HMRF) from the Food and Health Bureau of Hongkong (grant 10212456 to X.B.), and the 111 Project (grant B16021 to Z.Y.).

AUTHOR CONTRIBUTIONS

G.C., R.-R.H., Y.-F.L., W.-Y.S., Z.Y., M. Zhi, and J.Y. conceived this research. G.C., J.Y., Y.Z,. and Z.L. wrote the manuscript. J.Y., Y.Z., Z.G., J.M., S.L., and J.Z. carried out experiments and analyzed data. W.-Y.S., J.N., and H.G. performed redox phospholipidomics experiments. T.H. helped in the histological analysis of tissue slides, J.T. helped in ordering reagents, Q.W. helped in animal experiments, A.D. helped in flow cytometry. Z.L., X.B., J.J., M. Zhang, S.L., and G.S. helped in the discussion. G.C., R.-R.H., Y.-F.L., W.-Y.S., Z.Y., and M. Zhi mentored and supervised its participants.

DECLARATION OF INTERESTS

The authors declare no competing interests.

Received: June 14, 2024
Revised: July 12, 2024
Accepted: July 30, 2024
Published: August 17, 2024

REFERENCES

1. Kaplan, G.G., and Windsor, J.W. (2021). The four epidemiological stages in the global evolution of inflammatory bowel disease. Nat. Rev. Gastroenterol. Hepatol. *18*, 56–66. https://doi.org/10.1038/s41575-020-00360-x.
2. Agrawal, M., Allin, K.H., Petralia, F., Colombel, J.F., and Jess, T. (2022). Multiomics to elucidate inflammatory bowel disease risk factors and pathways. Nat. Rev. Gastroenterol. Hepatol. *19*, 399–409. https://doi.org/10.1038/s41575-022-00593-y.
3. Ho, G.T., and Theiss, A.L. (2022). Mitochondria and Inflammatory Bowel Diseases: Toward a Stratified Therapeutic Intervention. Annu. Rev. Physiol. *84*, 435–459. https://doi.org/10.1146/annurev-physiol-060821-083306.
4. Peloquin, J.M., Goel, G., Villablanca, E.J., and Xavier, R.J. (2016). Mechanisms of Pediatric Inflammatory Bowel Disease. Annu. Rev. Immunol. *34*, 31–64. https://doi.org/10.1146/annurev-immunol-032414-112151.
5. Khalili, H., Chan, S.S.M., Lochhead, P., Ananthakrishnan, A.N., Hart, A.R., and Chan, A.T. (2018). The role of diet in the aetiopathogenesis of inflammatory bowel disease. Nat. Rev. Gastroenterol. Hepatol. *15*, 525–535. https://doi.org/10.1038/s41575-018-0022-9.
6. Las Heras, V., Melgar, S., MacSharry, J., and Gahan, C.G.M. (2022). The Influence of the Western Diet on Microbiota and Gastrointestinal Immunity. Annu. Rev. Food Sci. Technol. *13*, 489–512. https://doi.org/10.1146/annurev-food-052720-011032.
7. Clough, J.N., Omer, O.S., Tasker, S., Lord, G.M., and Irving, P.M. (2020). Regulatory T-cell therapy in Crohn's disease: challenges and advances. Gut *69*, 942–952. https://doi.org/10.1136/gutjnl-2019-319850.
8. Whibley, N., Tucci, A., and Powrie, F. (2019). Regulatory T cell adaptation in the intestine and skin. Nat. Immunol. *20*, 386–396. https://doi.org/10.1038/s41590-019-0351-z.
9. Tanoue, T., Atarashi, K., and Honda, K. (2016). Development and maintenance of intestinal regulatory T cells. Nat. Rev. Immunol. *16*, 295–309. https://doi.org/10.1038/nri.2016.36.
10. Luck, H., Tsai, S., Chung, J., Clemente-Casares, X., Ghazarian, M., Revelo, X.S., Lei, H., Luk, C.T., Shi, S.Y., Surendra, A., et al. (2015). Regulation of obesity-related insulin resistance with gut anti-inflammatory agents. Cell Metab. *21*, 527–542. https://doi.org/10.1016/j.cmet.2015.03.001.
11. Newton, R., Priyadharshini, B., and Turka, L.A. (2016). Immunometabolism of regulatory T cells. Nat. Immunol. *17*, 618–625. https://doi.org/10.1038/ni.3466.

12. Bantug, G.R., Galluzzi, L., Kroemer, G., and Hess, C. (2018). The spectrum of T cell metabolism in health and disease. Nat. Rev. Immunol. *18*, 19–34. https://doi.org/10.1038/nri.2017.99.

13. Jiang, X., Stockwell, B.R., and Conrad, M. (2021). Ferroptosis: mechanisms, biology and role in disease. Nat. Rev. Mol. Cell Biol. *22*, 266–282. https://doi.org/10.1038/s41580-020-00324-8.

14. Seiler, A., Schneider, M., Förster, H., Roth, S., Wirth, E.K., Culmsee, C., Plesnila, N., Kremmer, E., Rådmark, O., Wurst, W., et al. (2008). Glutathione peroxidase 4 senses and translates oxidative stress into 12/15-lipoxygenase dependent- and AIF-mediated cell death. Cell Metab. *8*, 237–248. https://doi.org/10.1016/j.cmet.2008.07.005.

15. Yang, W.S., SriRamaratnam, R., Welsch, M.E., Shimada, K., Skouta, R., Viswanathan, V.S., Cheah, J.H., Clemons, P.A., Shamji, A.F., Clish, C.B., et al. (2014). Regulation of ferroptotic cancer cell death by GPX4. Cell *156*, 317–331. https://doi.org/10.1016/j.cell.2013.12.010.

16. Magtanong, L., Ko, P.J., and Dixon, S.J. (2016). Emerging roles for lipids in non-apoptotic cell death. Cell Death Differ. *23*, 1099–1109. https://doi.org/10.1038/cdd.2016.25.

17. Yang, W.S., Kim, K.J., Gaschler, M.M., Patel, M., Shchepinov, M.S., and Stockwell, B.R. (2016). Peroxidation of polyunsaturated fatty acids by lipoxygenases drives ferroptosis. Proc. Natl. Acad. Sci. USA *113*, E4966–E4975. https://doi.org/10.1073/pnas.1603244113.

18. Meyer, B.J., Mann, N.J., Lewis, J.L., Milligan, G.C., Sinclair, A.J., and Howe, P.R.C. (2003). Dietary intakes and food sources of omega-6 and omega-3 polyunsaturated fatty acids. Lipids *38*, 391–398. https://doi.org/10.1007/s11745-003-1074-0.

19. Mayr, L., Grabherr, F., Schwärzler, J., Reitmeier, I., Sommer, F., Gehmacher, T., Niederreiter, L., He, G.W., Ruder, B., Kunz, K.T.R., et al. (2020). Dietary lipids fuel GPX4-restricted enteritis resembling Crohn's disease. Nat. Commun. *11*, 1775. https://doi.org/10.1038/s41467-020-15646-6.

20. Schwarzler, J., Mayr, L., Vich Vila, A., Grabherr, F., Niederreiter, L., Philipp, M., Grander, C., Meyer, M., Jukic, A., Troger, S., et al. (2022). PUFA-Induced Metabolic Enteritis as a Fuel for Crohn's Disease. Gastroenterology *162*, 1690–1704. https://doi.org/10.1053/j.gastro.2022.01.004.

21. Zeng, H., Yang, K., Cloer, C., Neale, G., Vogel, P., and Chi, H. (2013). mTORC1 couples immune signals and metabolic programming to establish T(reg)-cell function. Nature *499*, 485–490. https://doi.org/10.1038/nature12297.

22. Ma, X., Xiao, L., Liu, L., Ye, L., Su, P., Bi, E., Wang, Q., Yang, M., Qian, J., and Yi, Q. (2021). CD36-mediated ferroptosis dampens intratumoral CD8(+) T cell effector function and impairs their antitumor ability. Cell Metab. *33*, 1001–1012.e5. https://doi.org/10.1016/j.cmet.2021.02.015.

23. Xu, S., Chaudhary, O., Rodriguez-Morales, P., Sun, X., Chen, D., Zappasodi, R., Xu, Z., Pinto, A.F.M., Williams, A., Schulze, I., et al. (2021). Uptake of oxidized lipids by the scavenger receptor CD36 promotes lipid peroxidation and dysfunction in CD8(+) T cells in tumors. Immunity *54*, 1561–1577.e1567. https://doi.org/10.1016/j.immuni.2021.05.003.

24. Pacella, I., Procaccini, C., Focaccetti, C., Miacci, S., Timperi, E., Faicchia, D., Severa, M., Rizzo, F., Coccia, E.M., Bonacina, F., et al. (2018). Fatty acid metabolism complements glycolysis in the selective regulatory T cell expansion during tumor growth. Proc. Natl. Acad. Sci. USA *115*, E6546-e6555. https://doi.org/10.1073/pnas.1720113115.

25. Kumagai, S., Togashi, Y., Sakai, C., Kawazoe, A., Kawazu, M., Ueno, T., Sato, E., Kuwata, T., Kinoshita, T., Yamamoto, M., et al. (2020). An Oncogenic Alteration Creates a Microenvironment that Promotes Tumor Progression by Conferring a Metabolic Advantage to Regulatory T Cells. Immunity *53*, 187–203.e8. https://doi.org/10.1016/j.immuni.2020.06.016.

26. Lim, S.A., Wei, J., Nguyen, T.L.M., Shi, H., Su, W., Palacios, G., Dhungana, Y., Chapman, N.M., Long, L., Saravia, J., et al. (2021). Lipid signalling enforces functional specialization of T(reg) cells in tumours. Nature *591*, 306–311. https://doi.org/10.1038/s41586-021-03235-6.

27. Matsushita, M., Freigang, S., Schneider, C., Conrad, M., Bornkamm, G.W., and Kopf, M. (2015). T cell lipid peroxidation induces ferroptosis and prevents immunity to infection. J. Exp. Med. *212*, 555–568. https://doi.org/10.1084/jem.20140857.

28. Ma, X., Hua, J., Mohamood, A.R., Hamad, A.R.A., Ravi, R., and Li, Z. (2007). A high-fat diet and regulatory T cells influence susceptibility to endotoxin-induced liver injury. Hepatology *46*, 1519–1529. https://doi.org/10.1002/hep.21823.

29. Deiuliis, J., Shah, Z., Shah, N., Needleman, B., Mikami, D., Narula, V., Perry, K., Hazey, J., Kampfrath, T., Kollengode, M., et al. (2011). Visceral adipose inflammation in obesity is associated with critical alterations in tregulatory cell numbers. PLoS One *6*, e16376. https://doi.org/10.1371/journal.pone.0016376.

30. Shaikh, S.R., MacIver, N.J., and Beck, M.A. (2022). Obesity Dysregulates the Immune Response to Influenza Infection and Vaccination Through Metabolic and Inflammatory Mechanisms. Annu. Rev. Nutr. *42*, 67–89. https://doi.org/10.1146/annurev-nutr-062320-115937.

31. Ringel, A.E., Drijvers, J.M., Baker, G.J., Catozzi, A., García-Cañaveras, J.C., Gassaway, B.M., Miller, B.C., Juneja, V.R., Nguyen, T.H., Joshi, S., et al. (2020). Obesity Shapes Metabolism in the Tumor Microenvironment to Suppress Anti-Tumor Immunity. Cell *183*, 1848–1866.e26. https://doi.org/10.1016/j.cell.2020.11.009.

32. Dyck, L., Prendeville, H., Raverdeau, M., Wilk, M.M., Loftus, R.M., Douglas, A., McCormack, J., Moran, B., Wilkinson, M., Mills, E.L., et al. (2022). Suppressive effects of the obese tumor microenvironment on CD8 T cell infiltration and effector function. J. Exp. Med. *219*, e20210042. https://doi.org/10.1084/jem.20210042.

33. Shaikh, S.R., Beck, M.A., Alwarawrah, Y., and MacIver, N.J. (2024). Emerging mechanisms of obesity-associated immune dysfunction. Nat. Rev. Endocrinol. *20*, 136–148. https://doi.org/10.1038/s41574-023-00932-2.

34. Yao, Y., Chen, Z., Zhang, H., Chen, C., Zeng, M., Yunis, J., Wei, Y., Wan, Y., Wang, N., Zhou, M., et al. (2021). Selenium-GPX4 axis protects follicular helper T cells from ferroptosis. Nat. Immunol. *22*, 1127–1139. https://doi.org/10.1038/s41590-021-00996-0.

35. Xu, C., Sun, S., Johnson, T., Qi, R., Zhang, S., Zhang, J., and Yang, K. (2021). The glutathione peroxidase Gpx4 prevents lipid peroxidation and ferroptosis to sustain Treg cell activation and suppression of antitumor immunity. Cell Rep. *35*, 109235. https://doi.org/10.1016/j.celrep.2021.109235.

36. Patankar, J.V., Müller, T.M., Kantham, S., Acera, M.G., Mascia, F., Scheibe, K., Mahapatro, M., Heichler, C., Yu, Y., Li, W., et al. (2021). E-type prostanoid receptor 4 drives resolution of intestinal inflammation by blocking epithelial necroptosis. Nat. Cell Biol. *23*, 796–807. https://doi.org/10.1038/s41556-021-00708-8.

37. Luo, X., Li, D.D., Li, Z.C., Li, Z.X., Zou, D.H., Huang, F., Wang, G., Wang, R., Cao, Y.F., Sun, W.Y., et al. (2024). Mitigating phospholipid peroxidation of macrophages in stress-induced tumor microenvironment by natural ALOX15/PEBP1 complex inhibitors. Phytomedicine *128*, 155475. https://doi.org/10.1016/j.phymed.2024.155475.

STAR★METHODS

KEY RESOURCES TABLE

REAGENT or RESOURCE	SOURCE	IDENTIFIER
Antibodies		
Brilliant Violet 421™ anti-mouse CD3ε	Biolegend	Cat#100335; RRID: AB_10898314
APC/Cyanine7 anti-mouse CD4	Biolegend	Cat#100414; RRID: AB_312699
PerCP/Cyanine5.5 anti-mouse CD8a	Biolegend	Cat#100734; RRID: AB_2075238
PE anti-mouse Ly-6G	Biolegend	Cat#127608 RRID: AB_1186099
APC anti-mouse CD11c	Biolegend	Cat#117310; RRID: AB_313779
PE anti-mouse/human CD11b	Biolegend	Cat#101208 RRID: AB_312791
APC anti-mouse CD36	Biolegend	Cat#102612 RRID: AB_2072639
eFluor™ 450 anti-FOXP3	Invitrogen	Cat#48-5773-82; RRID: AB_1518812
FITC anti-mouse IFN-γ	Biolegend	Cat#505806 RRID: AB_315400
PE/Cyanine7 anti-mouse IL-17A	Biolegend	Cat#506922 RRID: AB_2125010
PE anti-mouse CD25	Biolegend	Cat#113704 RRID: AB_2927943
Donkey Anti-Rabbit IgG H&L (Alexa Fluor® 680)	abcam	Cat#ab175772
Recombinant Anti-GPX4 antibody	abcam	Cat#ab125066
CD45 Polyclonal antibody	Proteintech	Cat#20103-1-AP RRID: AB_2716813
FITC Anti-Malondialdehyde antibody	abcam	Cat#ab27615
CD16/CD32 Monoclonal Antibody	Invitrogen	Cat#14-0161-81 RRID: AB_467133
InVivoMAb anti-mouse CD3ε	Bio X Cell	Cat#BE0001-1 RRID: AB_1107634
InVivoMab anti-mouse CD28	Bio X Cell	Cat#BE0015-1 RRID: AB_1107624
Chemicals, peptides, and recombinant proteins		
α-Tocotrienol (α-Toc)	Selleck Chemicals	Cat#E0191
Z-VAD-FMK (Z-VAD)	Selleck Chemicals	Cat#S7023
Necrostatin-1 (Nec-1)	Selleck Chemicals	Cat#S8037
Ferrostatin-1 (Fer-1)	Selleck Chemicals	Cat#S7243
BODIPY 581/591 C11	Invitrogen	Cat#D3861
Recombinant Murine IL-2	PeproTech	Cat#212-12
Recombinant Human TGF-β1	Novoprotein	Cat#CA59
Ionomycin	Beyotime	Cat#S1672
Phorbol 12-myristate 13-acetate	Sigma-Aldrich	Cat#P8139
BD GolgiStop	BD Biosciences	Cat#554724
Arachidonic Acid	Sigma-Aldrich	Cat#506-32-1

(*Continued on next page*)

Continued

REAGENT or RESOURCE	SOURCE	IDENTIFIER
Eicosapentaenoic Acid	Sigma-Aldrich	Cat#86227-47-6
linolenic acid	Sigma-Aldrich	Cat#463-40-1
linoleic acid	Sigma-Aldrich	Cat#60-33-3
Oleic acid	Sigma-Aldrich	Cat#112-80-1
anti-CD3/CD28 Dynabeads	Gibco	Cat#11456D
CellTrace™ Violet Cell Proliferation Kit	Invitrogen	Cat#C34571
Collagenase from Clostridium histolyticum IV	Sigma-Aldrich	Cat#C5138-5G
DNase I	Sigma-Aldrich	Cat#DN25-1G
FITC-Dextran (4kDa)	Sigma-Aldrich	Cat# 46944
Percoll	Cytiva	Cat#17089101
DPBS	Gibco	Cat#14190144
LIVE/DEAD™ Fixable Aqua Dead Cell Stain Kit	Invitrogen	Cat#L34966
SYBR Premix Ex TaqII	Takara	Cat#RR820A
RNA Isolation kit V2	Vazyme Biotech	Cat#RC112-01
TRIzol LS Reagent	Invitrogen	Cat#10296010CN
CellROX Green	Invitrogen	Cat#C10492
α-Tocotrienol	Sigma-Aldrich	Cat#90669-50G-F
Critical commercial assay kits		
EasySep™ Mouse Naive CD4+ T cell Isolation Kit	STEMCELL	Cat#19765
EasySep™ Mouse CD4+ T cell Isolation Kit	STEMCELL	Cat#19852
BD Cytofix/Cytoperm™ Fixation/ Permeabilization Kit	BD Biosciences	Cat#554714 RRID: AB_2869008
eBioscience™ Foxp3/Transcription Factor Staining Buffer Set	Invitrogen	Cat#00-5523-00
Mouse IL-1β ELISA Kit	Biolegend	Cat#432604
Mouse IL-6 ELISA Kit	Biolegend	Cat#431304
Mouse TNF-α ELISA Kit	Biolegend	Cat#430904
GSH and GSSG Assay Kit	ABclonal	Cat#RK05819
LDH Cytotoxicity Assay Kit	Beyotime	Cat#C0017
Triglyceride enzymatic liquid sample determination kit	APPLYGEN	Cat#E1003
lipoprotein very low-density lipoprotein cholesterol (LDLVLDL-C) enzymatic assay kit	APPLYGEN	Cat#E1018
Blood high-density lipoprotein cholesterol (HDL-C) enzymatic assay kit	APPLYGEN	Cat#E1017
Experimental models: Organisms/strains		
Mouse: *Gpx4*$^{tm1.1Qra}$/J	The Jackson Laboratory	Strain #: 027964 RRID: IMSR_JAX:027964
Mouse: B6.129(Cg)-*Foxp3*$^{tm4(YFP/icre)Ayr}$/J	The Jackson Laboratory	Strain #: 016959 RRID: IMSR_JAX:016959
Mouse: B6.129S7-*Rag1*^{tm1Mom}/J	The Jackson Laboratory	Strain #: 002216 RRID: IMSR_JAX:002216
Mouse: B6.SJL-*Ptprc*^{a} *Pepc*^{b}/BoyJ (CD45.1)	The Jackson Laboratory	Strain #:002014 RRID: IMSR_JAX:002014
Mouse: C57BL/6J	The Jackson Laboratory	Strain #:000664 RRID: IMSR_JAX:000664

(*Continued on next page*)

Continued

REAGENT or RESOURCE	SOURCE	IDENTIFIER
Oligonucleotides		
Mouse *Gapdh*-forward 5′-ATCATCCCTGCATCCACT-3′	This paper	N/A
Mouse *Gapdh*-reverse 5′-ATCCACGACGGACACATT-3′	This paper	N/A
Mouse *Cldn1*-forward 5′-TTGGCAGCTCTTTCTGGTGT-3′	This paper	N/A
Mouse *Cldn1*-reverse 5′-ACAGCTTGCATGCTGTCTCA-3′	This paper	N/A
Mouse *Muc2*-forward 5′-GGCTGGAGTGACTCTGAACTATG-3′	This paper	N/A
Mouse *Muc2*-reverse 5′-GAGTGCAGCGTAACTTCCATTGT-3′	This paper	N/A
Mouse *Ocln*-forward 5′-AGGGAGATGACGTGCTCCC-3′	This paper	N/A
Mouse *Ocln*-reverse 5′-CCGTTTCCCGTAGCGGTTA-3′	This paper	N/A
Mouse *Zo1*-forward 5′-CGAGGCATCATCCCAAATAAGAAC-3′	This paper	N/A
Mouse *Zo1*-reverse 5′-TCCAGAAGTCTGCCCGATCAC-3′	This paper	N/A
Mouse *Il1b*-forward 5′-GCATGGACCTGAGTTCTGGTG-3′	This paper	N/A
Mouse *Il1b*-reverse 5′-AGGCCACAGGTATTTTGTCG-3′	This paper	N/A
Mouse *Il23*-forward 5′-CCTTGGGGTCCTCACTGGA-3′	This paper	N/A
Mouse *Il23*-reverse 5′-TTGGCCAGGTCCTCAGTTTCC-3′	This paper	N/A
Mouse *Tnf*-forward 5′-CCCTCACACTCAGATCATCTTC-3′	This paper	N/A
Mouse *Tnf*-reverse 5′-GCTACGACGTGGGCTACAG-3′	This paper	N/A
Mouse *Cxcl1*-forward 5′-TTGCCAATGAGGAAGTCAGA-3′	This paper	N/A
Mouse *Cxcl1*-reverse 5′-TTCTTCCGTTACTTGGGGAC-3′	This paper	N/A
Mouse *Mcp1*-forward 5′-AGGTCCCTGTCATGCTTCTG-3′	This paper	N/A
Mouse *Mcp1*-reverse 5′-TTGGGACACCTTTTAGCATC-3′	This paper	N/A
Other		
NCD with deprivation of vitamin E	HFKbio	Cat#AIN-96G Custom diets
High fat diet (HFD)	Reserche Diets	Cat#D12492
Normal chew diet (NCD)	Jiangsu Xietong Pharmaceutical Bio-engineering	Cat#1010058
Software and algorithms		
FlowJo (v10.8)	TreeStar	https://www.flowjo.com/
Prism (v9)	GraphPad	https://www.graphpad.com/
Compound Discoverer 2.0	Thermo Fisher Scientific	https://mycompounddiscoverer.com/

RESOURCE AVAILABILITY

Lead contact

Further information and requests for resources and reagents should be directed to and will be fulfilled by the lead contact, Guangchao Cao (gccao2016@jnu.edu.cn).

Materials availability

All materials are available from the lead contact upon request.

Data and code availability

- All data reported in this paper will be shared by the lead contact upon request.
- This paper does not report original code.
- Any additional information required to reanalyze the data reported in this work paper is available from the lead contact upon request.

EXPERIMENTAL MODEL AND STUDY PARTICIPANT DETAILS

Mice

Gpx4$^{tm1.1Qra}$/J (*Gpx4*$^{flox/flox}$, strain #027964), B6.129(Cg)-*Foxp3*$^{tm4(YFP/icre)Ayr}$/J (*Foxp3*$^{YFP-Cre}$, strain #016959), B6.129S7-*Rag1*^{tm1Mom}/J (strain #002216), B6.SJL-*Ptprc*^{a} *Pepc*^{b}/BoyJ (CD45.1, strain #002014) and C57BL/6J (Strain #000664) mice strains were purchased from the Jackson Laboratory and housed in SPF conditions in the Laboratory Animal Center of Jinan University. *Gpx4*$^{flox/flox}$ and *Foxp3*$^{YFP-Cre}$ strains were crossed to generate Tregs-specific GPX4 deficient *Foxp3*$^{YFP-cre}$ *Gpx4*$^{f/f}$ (KO) mice, age and sex matched *Foxp3*$^{YFP-Cre}$ mice (WT) were used as controls. Male mice at 6–8 weeks of age were used for the treatment by normal chew diet (NCD), high fat diet (HFD), NCD with deprivation of vitamin E or NCD supplemented with α-Tocopherol for indicated time and then sacrificed for analysis. Animal procedures were approved by the Institutional Laboratory Animal Care and Use Committee of Jinan University.

METHOD DETAILS

Lamina propria lymphocytes isolation

Payer's patches in small intestines were removed. Small intestine or colon tissue were dissected and cut into pieces. The epithelial layers were removed by sequential incubation with DTT (1 mM) and EDTA (5 mM) in PBS for 10 min each. The remaining tissue were digested with collagenase (type VIII, 1 mg/mL) and DNase I (300 μg/mL) in prewarmed RPMI1640 medium at 37°C for 40 min and then shaken vigorously to yield cell suspension. The debris were removed by 70μm cell strainer. The total lamina propria lymphocytes were purified on an 40/80% Percoll gradient.

Flow cytometry

Cell suspensions were washed twice in PBS. Anti-CD16/CD32 Abs were used for Fc receptor blocking. For the staining of cell surface proteins, fluorescein conjugated antibodies were added in the suspensions and incubated at 4°C for 15 min. For intracellular cytokine staining, lymphocytes were stimulated with Phorbol 12-myristate 13-acetate (PMA, 50 ng/mL) and ionomycin (1 μg/mL) in the presence of GolgiStop for 4–6 h. Cells were then fixed and permeabilized using BD Cytofix/Cytoperm Fixation/Permeabilization Kit, and stained with fluorescein conjugated anti-cytokine Abs in the Perm/Wash buffer. Intra-nuclear Foxp3 was stained using the eBioscience Foxp3/Transcription Factor Staining Buffer Set. Anti-GPX4 rabbit primary antibody and fluorescein conjugated anti-rabbit secondary antibody were used to detect intracellular GPX4 expression level. BODIPY 581/591 C11 and anti-malondialdehyde (MDA) Abs were used to detect lipid peroxidation. Cellrox green was used to detect reactive oxygen species production. Cell death was detected using LIVE/DEAD or 7-AAD. Flow cytometry was performed on BD FACSVerse or Cytek NL-CLC and data were analyzed using FlowJo (v10.8).

Histology

Heart or colon tissues from mice were obtained, fixed in paraformaldehyde (4%) and embedded in paraffin. Sections (4 mm thick) that had been deparaffinized and rehydrated were stained with hematoxylin and eosin (H&E). For the detection of immunocytes infiltration, immunohistochemical staining of CD45 was performed. Alcian blue or the combined staining of Alcian blue and Periodic Acid Schiff (AB-PAS) was used for the detection of mucin.

Quantitative real-time PCR

Total RNA was isolated using TRIzol LS Reagent and cDNA was obtained with Takara Reverse Ttranscription Kit. Real-time quantitative PCR was performed using SYBR Premix Ex TaqII and LightCycler480 II,384 (Roche). All runs were accompanied by the internal control gene *Gapdh*. The samples were run in triplicate and normalized to *Gapdh* using the $2^{-}\Delta\Delta Ct$ method to provide arbitrary units representing relative expression levels. The primer sequences are listed in the Key resource table.

In vitro activation of T cells

CD4$^+$ T Cells were enriched from the spleen of *Gpx4*$^{+/+}$ *Foxp3*$^{YFP-cre}$ (WT) or *Gpx4*$^{f/f}$ *Foxp3*$^{YFP-cre}$ (KO) mice using EasySep Mouse CD4$^+$ T cell isolation kit according to the manufacturer's instructions. Enriched CD4$^+$ T Cells (3 x 10^6 cells/ml) were treated with plate bound anti-CD3ε Abs (10 μg/mL), soluble anti-CD28 Abs (1 μg/mL) and rmIL-2 (2 ng/mL) in RPMI-1640 media supplemented with 10% FBS for indicated time at 37°C. Unstimulated groups was also performed. For some experiments, the following small molecule inhibitors were added during the activation of T cells: a-tocopherol (aToc, 10μM), z-VAD-FMK (20μM), Necrostatin-1 (Nec-1, 20μM), Ferrostatin-1 (Fer-1, 20μM). For the detection of death rates or survival rates in YFP+ Treg cells or YFP- Tconv cells after treatment, cells were collected and stained with LIVE/DEAD. For the detection of lipid peroxidation, cells were fixed and permeabilized using the eBioscience Foxp3/Transcription Factor Staining Buffer Set (YFP was denatured and lost fluorescence after fixation), and stained for FOXP3, MDA and Bodipy.

In vitro fatty acid treatment

CD4$^+$ T cells enriched from the spleen of *Foxp3*$^{YFP-cre}$ (WT) mice were adjusted to 3×10^6 cells/mL and treated with individual fatty acid (Oleic acid, linoleic acid, linolenic acid, eicosapentaenoic acid, arachidonic acid, docosahexaenoic acid) at 160μM. Ethanol was used as vehicle for the addition of arachidonic acid and the final concentration of ethanol in the culture medium was about 0.1%. After 48h, the death rate in YFP+ Treg cells or YFP- Tconv cells were detected by LIVE/DEAD (Figures S2A and S2B). CD4$^+$ T cells were also treated with different dose of oleic acid (OA) or arachidonic acid (AA) for 48h, the death rate and lipid peroxidation in Treg cells were detected by LIVE/DEAD and BODIPY 581/591 C11 respectively (Figure 2E). For the rescue of AA-induced ferroptosis, CD4$^+$ T cells were treated with AA (40μM) in the presence or absence of Fer-1 (20μM) for 48h, the death rate, lipid peroxidation and glutathione ratios in Treg cells were detected (Figures 2F, 2G and S2C).

Suppression assay of treg cells

Naive CD4$^+$ T cells from the spleen of CD45.1 strain mice were purified using EasySep Mouse Naive CD4$^+$ T cell Isolation Kit and labeled with 5mM CellTrace Violet according to the manufacturer's instructions. Treg cells (CD4$^+$ YFP$^+$) from the spleen of *Foxp3*$^{YFP-Cre}$ or *Foxp3*$^{YFP-Cre}$ *Gpx4*$^{f/f}$ mice (CD45.2 background) were sorted using flow cytometry. For *in vitro* immunosuppression assay, Naive CD4$^+$ T cells were co-cultured with Treg cells in U 96-well plate at indicated ratios with the stimulation of anti-CD3/CD28 Dynabeads. After 3 days of co-culture, CD45.1$^+$ CD4$^+$ T cells were detected for Cell Trace Violet dilution by flow cytometry. For *in vivo* immunosuppression assay, Rag1$^{-/-}$ mice were *i.v.* injected with a mixture of 4×10^5 Naive CD45.1$^+$ CD4$^+$ T cells and 2×10^5 Tregs. Mice were weighed every week for 6 weeks and then euthanized for tissue harvest and analysis.

Preparation of treg cells for lipidomic analysis

CD4$^+$ T cells from the spleens of *Foxp3*$^{YFP-Cre}$ mice were collected using EasySep Mouse CD4$^+$ T cell Isolation Kit, and CD4$^+$T cells were cultured for 3 days under the conditions with plate-coated anti-CD3 (10 μg/ml), anti-CD28 (10 μg/ml), TGF-β (5 μg/ml) and IL-2 (2 ng/ml) for inducing Treg cells or plate-coated anti-CD3 (10 μg/ml), anti-CD28 (10 μg/ml) and IL-2 (2 ng/ml) for Tconv cells. Then, cells were expanded for another 3 days with TGF-β (5 μg/ml) and IL-2 (2 ng/ml) for Treg or IL-2 (2 ng/ml) only for Tconv. YFP$^+$ Treg cells from Treg culturing condition and YFP- Tconv cells from Tconv culture condition were sorted using BD FACS AriaII (BD Biosciences). Purified YFP$^+$ Treg cells and YFP- Tconv cells were then treated with AA (40μM) or OA (40μM) for 48h (5×10^6 cells in each group), and then washed with normal saline solution before LC-MS/MS-based phospholipidomics analysis.

For the comparison between GPX4 deficient and sufficient Treg cells, CD4$^+$ YFP+ Treg cells were sorted from the freshly isolated splenocytes of *Foxp3*$^{YFP-Cre}$ *Gpx4*$^{f/f}$ (KO) and *Foxp3*$^{YFP-Cre}$ (WT) mice and directly used for LC-MS/MS-based phospholipidomic and redox phospholipidomic analysis. Each sample of Treg cells were pooled from 5 to 10 mice.

LC-MS/MS-based phospholipidomics analysis

The preparation and analysis of phospholipids were conducted as previously described.[37] A Dionex UltiMate 3000 DGLC standard system (Thermo Fisher Scientific, MA, USA) with an HILIC column (2.1 mm × 100 mm, 1.7 μm, Waters, Milford, MA, USA) was utilized for phospholipid separation. Solvent A consisted of acetonitrile:water (95:5,v/v), while solvent B was acetonitrile:water (50:50,v/v) containing 10 mM ammonium formate as mobile-phase modifiers. The gradient elution program was as follows: 0–10 min, 35% solvent B; 10.1–13 min, hold at 100% solvent B; 13.1–22 min, hold at 0% solvent B for equilibration. The flow rate was set at 0.25 mL/min, and the column temperature was maintained at 40°C. Ion source conditions were configured as follows: spray voltage set to 2.8 kV; capillary temperature maintained at 350°C; auxiliary gas heater temperature set to 320°C; S-lens Rf level at 65; sheath gas flow at 30 (arbitrary units); and auxiliary gas flow at 15 (arbitrary units). Phospholipids were detected using a Q Exactive mass spectrometer (Thermo Fisher Scientific, MA, USA) and analyzed with Compound Discoverer 2.0 (Thermo Fisher Scientific, MA, USA) using an in-house generated analysis workflow. Phospholipid species were identified and filtered based on their retention time.

QUANTIFICATION AND STATISTICAL ANALYSIS

GraphPad Prism were used for statistical analysis and calculated p values. Data are presented as the mean ± sd. The statistical details of experiments can be found in the figure legends. Each dot in the figure represents a biological independent sample unless otherwise stated. Two-tailed unpaired Student's t-test were used to compare differences between two groups. Log rank test was used for survival curve analysis. For analysis among three or more groups, one-way ANOVA was used. For analyzing data involving two independent parameters, two-way ANOVA was used. $p < 0.05$ (*), $p < 0.01$ (**) and $p < 0.001$ (***) indicate statistically significant changes. NS, not significant.